OPEN ACCESS
Journal of Medical Robotics Research, Vol. 7, Nos. 2 & 3 (2022) 2241007 (13 pages)
© The Author(s)
DOI: 10.1142/S2424905X22410070

Journal of Medical Robotics Research
https://www.worldscientific.com/worldscinet/jmrr

Journal of Medical Robotics Research

J. Med. Robot. Res. 2022.07. Downloaded from www.worldscientific.com
by KATHOLIEKE UNIVERSITEIT LEUVEN on 10/10/22. Re-use and distribution is strictly not permitted, except for Open Access articles.

Concentric Dual-Chamber Pneumatic Artificial Muscles: Miniature Actuators Designed for Use in Minimally Invasive Surgical Instruments

Robert Lathrop*,‡, Mouloud Ourak*, Jan Deprest†, Emmanuel Vander Poorten*

*Mechanical Engineering Department
KU Leuven, Celestijnenlaan 300B, 3001 Leuven, Belgium

†Department of Obstetrics and Gynecology
UZ Leuven, Herestraat 49, 3000 Leuven, Belgium

Development of high-performance flexible surgical instruments is important to simplify and enable new minimally invasive surgical procedures. New actuation technologies are necessary to produce flexible instrumentation that is capable of accessing difficult-to-reach anatomy and performing laborious tasks without damaging delicate tissues. Recently, concentric McKibben muscles and dual-chamber pneumatic artificial muscles (PAMs) have been proposed for use in miniature flexible robotic surgical instrumentation. In this study, several varieties of a hybrid concentric dual-chamber PAM design are built and their force generation and stroke length are compared to a contractile McKibben muscle. The concentric dual-chamber PAM is designed to provide surgical access for large diameter (1.5–2.0 mm) instruments to be delivered to the surgical site in a pneumatically sealed actuator suitable for miniaturization and integration into surgical devices used in fluid environments (fetal applications in particular). Force output of the concentric dual-chamber PAM is modeled and compared to experimental results. Initial results suggest that the newly introduced design produces a higher actuation force per unit length than traditional McKibben muscles. The prototype dual-channel PAM produced a maximum 15.25 N of force and 8.39 mm of stroke, in comparison to 13.31 N of force and 19.3 mm of stroke produced by a traditional contractile McKibben muscle of the same length, outer diameter, and materials.

Keywords: Actuator design; minimally invasive surgery; mechanisms for robots; flexible devices.

JMRR

1. Introduction

1.1. *Clinical background*

The ongoing development of surgical robotic systems has driven a need for new actuation technologies that are capable of providing relatively high output forces and precise positional control in a minimal physical footprint. To expand indications for new minimally invasive surgery (MIS) procedures, it is important to develop robotic instrumentation that will enable surgeons to accurately navigate complex anatomy and perform laborious tasks on delicate tissue structures. One MIS procedure that has been identified as a promising target for simplification by robotic instrumentation is Fetoscopic Endoluminal Tracheal Occlusion (FETO). FETO involves the in-utero placement of an inflatable balloon in the trachea of a 27–32 week old fetus [1]. A second intervention is then performed at 34 weeks (or earlier if indicated) to deflate and remove the balloon, which frees the airway and induces lung maturation [2]. An illustration showing a fetoscope being used to access the fetal trachea during a FETO procedure is shown in Fig. 1. Using current rigid

Received 7 December 2021; Revised 28 July 2022; Accepted 31 July 2022; Published 21 September 2022. Published in JMRR Special Issue on ISMR 2021. Guest Editor: Iulian Ioan Iordachita.
Email Address: ‡*Bob.Lathrop@KULeuven.be*
NOTICE: Prior to using any material contained in this paper, the users are advised to consult with the individual paper author(s) regarding the material contained in this paper, including but not limited to, their specific design(s) and recommendation(s).

This is an Open Access article published by World Scientific Publishing Company. It is distributed under the terms of the Creative Commons Attribution 4.0 (CC BY) License which permits use, distribution and reproduction in any medium, provided the original work is properly cited.

J. Med. Robot. Res. 2022.07. Downloaded from www.worldscientific.com
by KATHOLIEKE UNIVERSITEIT LEUVEN on 10/10/22. Re-use and distribution is strictly not permitted, except for Open Access articles.

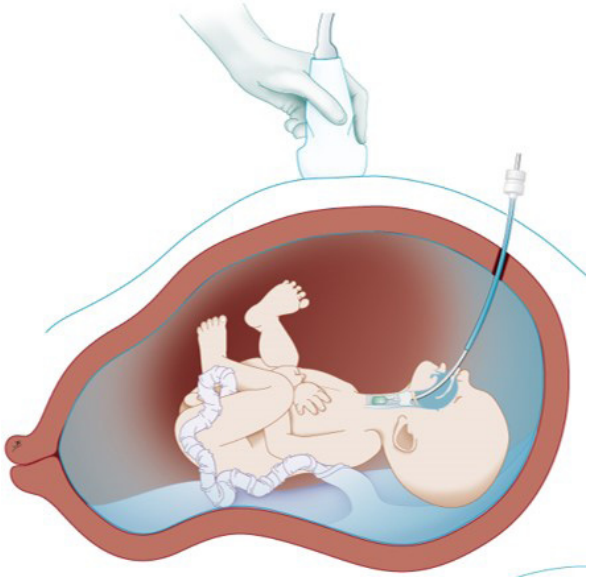

Fig. 1. Illustration of a fetoscope being used to access the fetal trachea under ultrasound guidance during a FETO procedure.

instrumentation it is necessary to have an unobstructed path from the surgical incision in the mother's abdomen to the mouth of the fetus. This access can be challenging or at times impossible to achieve given the mobility of the fetus, the location of the placenta within the womb and the difficulty of changing the fetus' position or orientation during the procedure.

Flexible surgical instrumentation could be advantageous to help overcome these challenges and enable a wider range of surgeons to more easily perform FETO procedures. Miniaturization forms another important consideration for devices designed for fetal surgery due to the observed increase in membrane rupture rates following fetal procedures performed with larger diameter instruments [3].

1.2. *Flexible fetoscope design requirements*

The below list of design requirements for a flexible fetoscope designed specifically for FETO procedures was developed through a mix of physician feedback, case observation, and literature review.

(1) Device provides camera or fiber optic visualization, illumination, and saline delivery comparable to current state of the art.
(2) Device outer diameter ≤ 3.3 mm to fit within footprint of existing fetoscopes.
(3) Device working channel (WC) ≥ 1.75 mm to enable passage of 1.65 mm diameter uninflated balloon.
(4) Device is capable of providing sufficient actuation force and stroke to articulate the bending arm 90° over a length of 40 mm to enable access to the fetal trachea from the fetal mouth.
(5) Device is compliant in the bending axis to enable safe maneuvering into the fetal trachea, but rigid enough in the nonbending axis to enable the surgeon to reposition the fetus' body with the fetoscope.
(6) Device enables fetal trachea access from a wider range of initial incisions. Based on surgeon feedback initial devices will be built with one uniaxial degree of freedom (DOF) to allow the device tip to conform to the fetal trachea. More complex devices with additional DOF will be investigated if this is not sufficient.

This paper will explore the development of a novel pneumatic actuator intended for integration in a flexible fetoscope that meets the above criteria and evaluate the proposed actuator design coupled with a tool guide designed for use in a flexible fetoscope.

1.3. *Pneumatic artificial muscle actuators*

A key aspect of designing small diameter flexible surgical instrumentation is the development of new miniature actuators capable of precisely delivering high forces through devices which may need to articulate around delicate anatomic structures to reach the surgical intervention site. Pneumatic artificial muscles (PAMs, an air-driven subset of fluidic artificial muscle) are an ideal actuator variety for flexible surgical instruments due to their high power-to-weight ratio, inherent compliance, and high response bandwidth [4, 5]. PAMs were originally developed for prosthetic applications by Joseph McKibben in the 1950s [6]. After being patented by Gaylord in 1958 [7], PAMs have been developed for a wide range of aerospace, healthcare, and industrial robotics applications [8–10]. In addition to the previously mentioned benefits their appeal is due in part to their simple construction. PAMs are composed of an elastic bladder enclosed by a braided mesh of inextensible fibers. The bladder and mesh are fixed into end connectors at either end and pneumatically sealed. This assembly is then driven by an external pressure source. As pressure inside the PAM increases the elastic bladder expands, transferring force to the inextensible fibers and generating an axial force. The direction of this force is dictated by the braided mesh geometry.

As illustrated in Fig. 2, if the angle between the braid fibers and the long axis of the muscle at rest is greater than 54.44° the muscle will extend axially and contract radially, producing an axial force in the extensile direction as the braid angle increases toward 54.44°. A braid angle below 54.44° will produce a PAM that responds to an increase in pressure by contracting axially and expanding radially, producing a contractile axial force as the braid angle decreases toward 54.44° [11]. Contractile PAMs are often favored over extensile due to their higher force generation (up to 10 times greater than extensile)

J. Med. Robot. Res. 2022.07. Downloaded from www.worldscientific.com
by KATHOLIEKE UNIVERSITEIT LEUVEN on 10/10/22. Re-use and distribution is strictly not permitted, except for Open Access articles.

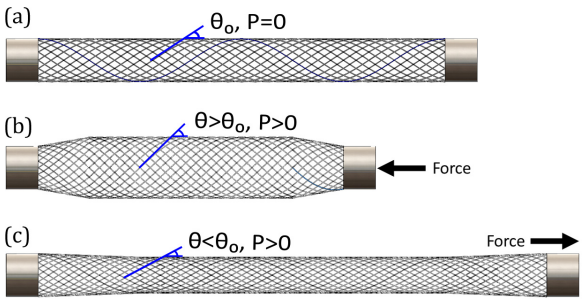

Fig. 2. Working principle of a PAM showing (a) unpressurized PAM at rest (pressure $P = 0$, resting braid angle $= \theta_0$), (b) contractile PAM with initial braid angle $\theta < 54.44°$ contracting axially as pressure increases and (c) extensile PAM with initial braid angle $\theta > 54.44°$ extending axially as pressure increases.

[12], but there have also been robotic applications where extensile PAMs were favored due to their higher potential stroke length [13].

Recently new actuator designs have been introduced to produce PAMs more suitable for integration in miniature surgical devices, including concentric PAMs [14] and dual-chamber PAMs [15]. Concentric PAMs make use of the empty space within the center of the muscle to include an integrated WC that can be used to introduce tools to the surgical environment. As shown in Figs. 3(a) and 3(b), one end of the concentric PAM is fixed relative to the concentric WC while the other end translates over the channel over the course of actuation. This interface between the translating endpoint and the WC can be difficult to seal, especially in actuators with small elastic bladder diameter and relatively large WC diameter. The addition of a piston seal or similar component would increase actuator diameter as well as increasing the friction between the traveling endpoint and WC under pressurization, which could reduce force generation and increase the actuator's output hysteresis.

Dual-chamber concentric PAMs provide similar functionality to concentric PAMs with improved pneumatic sealing and force generation. A dual-chamber PAM consists of a contractile and extensile PAM pneumatically connected in series. As shown in Figs. 3(c) and 3(d), this provides fixed endpoints at both ends of the actuator which enables easier pneumatic sealing of devices with a relatively large concentric WC and relatively small overall device diameter. The dual-channel PAM uses a traveling connection point in between the muscles to transmit force to the target component (for example, the bending segment of a flexible surgical instrument). Because the actuator is pneumatically sealed at the fixed endpoints proximal and distal to the traveling connection point, there is no need for a pneumatic seal that moves with the traveling connection point. The dual-chamber PAM is also shown in this study to produce a higher actuation force than a pure contractile PAM of the same length. Two potential flexible fetoscope designs using dual-chamber concentric PAMs are illustrated in Fig. 4. A shaft-embedded dual-chamber PAM is shown in Figs. 4(a)–4(d), in which the PAM is enclosed in a laser cut nitinol tool guide at the distal tip of the fetoscope. An asymmetric pattern is used to bias the tool guide to bend uniaxially. As seen in Fig. 4(b), the right side of the guide is cut into a bending pattern, while the left side is cut into a driving arm that is fixed to the traveling attachment point of the dual-chamber PAM. The chambers of the PAM are also rigidly fixed to the proximal and distal attachment points. Once pressurized the traveling attachment point will advance distally, causing the tool guide to bend to the desired orientation. A second implementa-

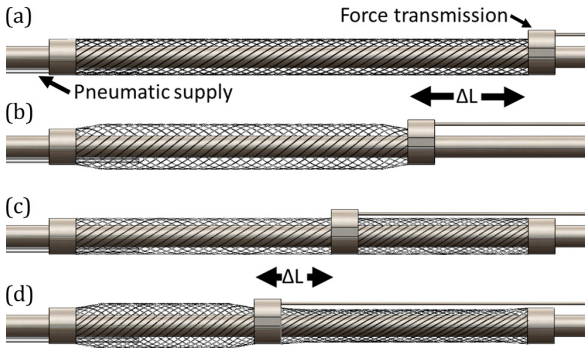

Fig. 3. Comparison of the response to pressurization by different concentric PAM varieties (a) concentric PAM at rest ($P = 0$); (b) concentric PAM pressurized and contracting; (c) dual-chamber concentric PAM at rest ($P = 0$); (d) dual-chamber concentric PAM when pressurized.

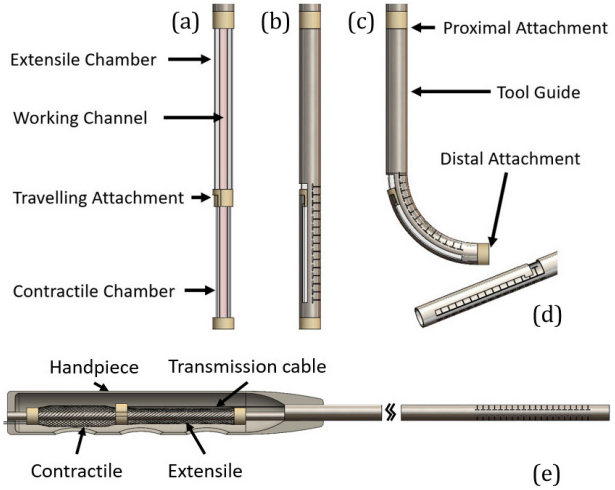

Fig. 4. Illustration showing two potential implementations for a flexible fetoscope actuated by a dual-chamber concentric PAM. In (a)–(d) the actuator is embedded in the shaft of a flexible fetoscope, including (a) interior view of chambers with tool guide removed, (b) exterior view of shaft-embedded dual-chamber PAM, (c) view of pressurized PAM articulating the device tip, and (d) isolated view of the tool guide, rotated to show asymmetric cut pattern. (e) Depicts a handpiece-embedded actuator using a cable to transmit force to the device tip.

J. Med. Robot. Res. 2022.07. Downloaded from www.worldscientific.com
by KATHOLIEKE UNIVERSITEIT LEUVEN on 10/10/22. Re-use and distribution is strictly not permitted, except for Open Access articles.

tion is shown in Fig. 4(e), in which the actuator is embedded in the handpiece of a surgical instrument and a cable is used to transmit force from the actuator to the device tip. This configuration enables the use of larger diameter PAMs with higher force output than the shaft-embedded implementation.

This study reports on the first ever concentric dual-chamber PAM with integrated WC and introduces experiments conducted to characterize its output in comparison to a traditional contractile McKibben muscle and a dual-chamber PAM with no integrated WC and compares PAM performance to its theoretically modeled behavior.

2. Methods and Materials

2.1. *Basic modeling of PAMs*

Many different approaches have been developed to model the force output of contractile [7, 11, 16–22] and extensile [12, 23] PAMs. The method used in this paper is based on the force balance method derived by Kothera *et al.* [17], a linear elastic model that was developed by assuming balanced forces in the free body diagram of a PAM undergoing actuation. The model proposed by Kothera *et al.* is

$$F = \frac{P}{4N^2\pi}(3L^2 - B^2) + P\left(\frac{V_b}{L} - \frac{tL^2}{2\pi RN^2}\right) + E_r V_b\left(\frac{1}{L_0} - \frac{1}{L}\right) + \frac{E_r L}{2\pi RN^2}(tL - t_0 L_0), \quad (1)$$

wherein F is the force exerted by the actuator, P is the actuation pressure driving the PAM, N is the number of turns the braid strands make along the length of the PAM, L is actuator length as a function of pressure, B is the length of each braid strand, V_B is the volume of the elastic bladder material, t is the elastic bladder thickness as a function of pressure, R is the bladder radius, E_r is the elastic modulus of the elastic bladder material, L_0 is the initial length of the PAM, and t_0 is the initial thickness of the elastic bladder.

To model the PAM's blocked force the assumption was made that PAM length (and consequently bladder thickness and bladder material volume) remained constant during testing. A term P_{DB} was also introduced to account for dead-band pressure, as has been used in several previous PAM models [4, 18, 24]. The dead-band pressure accounts for the amount of pressure that must be delivered to the actuator before it is able to produce an output force. This is commonly visualized as the pressure required to inflate the elastic bladder to the point that it is braced against the fibers of the inelastic braid. For the purposes of this study dead-band pressure was defined for each prototype as the experimentally measured pressure at which the prototype's force output surpasses a threshold of 0.2 N. Under these assumptions the model proposed by Kothera *et al.* takes the form used in this study to model actuator output force

$$F = \frac{P - P_{DB}}{4N^2\pi}(3L^2 - B^2) + (P - P_{DB})\left(\frac{V_b}{L} - \frac{tL^2}{2\pi RN^2}\right). \quad (2)$$

2.2. *Modeling of a dual-chamber concentric PAM*

Each dual-chamber PAM comprises two segments, one constructed using a mesh with a braid angle below 54.44° that will contract when pressurized and one from a mesh with a braid angle above 54.44° that will extend when pressurized. The prototypes constructed in this study have separate elastic bladders in each chamber that are pneumatically connected in series. Given that air is able to flow between chambers with minimal restriction, it is assumed that the pressure in both chambers is equal and that this is equal to the pressure supplied in this study by a proportional valve. Both chambers are connected at a traveling attachment point that is used to transmit force generated by the chambers out to the actuation target. The forces generated by these chambers are visualized in Fig. 5. To model the force output delivered to the traveling attachment point by the dual-chamber prototypes their chambers were each modeled as separate PAMs. Relying on the modified Kothera model of (2) this leads then to a force output

$$F_{\text{dual-chamber}} = F_{\text{contractile}} + \text{abs}(F_{\text{extensile}}). \quad (3)$$

Note that the absolute value of the extensile chamber's force contribution is used because though the extensile PAM force calculation will always be negative, it is oriented in the dual-chamber PAM design such that it will be pushing the traveling attachment point in the same direction that the contractile PAM pulls the attachment point (as shown in Fig. 5).

2.3. *Miniature PAM prototypes for comparison*

In order to evaluate the performance of the proposed design in comparison to existing PAM designs four prototypes were constructed: two dual-chamber PAMs with integrated WC (Fig. 6(a)), a dual-chamber PAM with no WC (Fig. 6(b)), and a contractile muscle with the same overall length as the dual-chamber PAMs (Fig. 6(c)). One dual-chamber prototype included a 1.9 mm outer diameter WC, while the other contained a WC with 1.5 mm outer diameter. The dual-chamber contractile chambers were each 80 mm in working length (not including connector pieces) while the extensile chambers were 50 mm each. The contractile-only prototype was 130 mm in working length.

The connector pieces for all prototypes were printed from an ABS resin using a Prusa SL1 machine (Prague,

J. Med. Robot. Res. 2022.07. Downloaded from www.worldscientific.com
by KATHOLIEKE UNIVERSITEIT LEUVEN on 10/10/22. Re-use and distribution is strictly not permitted, except for Open Access articles.

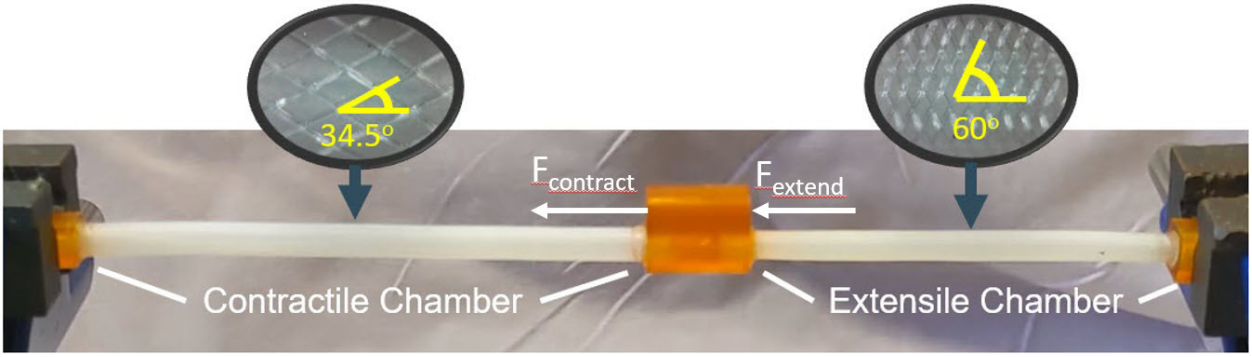

Fig. 5. Assembled dual-chamber PAM. The contractile and extensile chambers are built from the same materials, differing only in braid angle. Both chambers are driven by the same pneumatic supply channel.

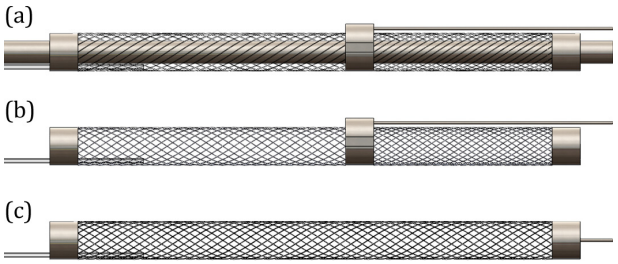

Fig. 6. Prototypes tested in this study (a) dual-chamber PAM with concentric WC; (b) dual-chamber PAM without WC; (c) contractile McKibben muscle.

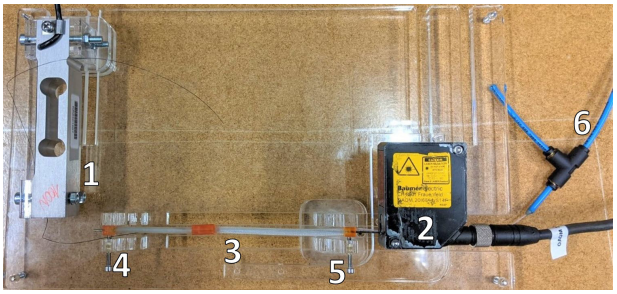

Fig. 7. Test setup used for prototype characterization, including (1) load cell, (2) distance sensor, (3) prototype, (4) distal clamping piece, (5) proximal clamping piece, (6) pneumatic connection to pressure sensor and pressure regulator.

Czechia). Silicone tubing (Dow Corning, Michigan, USA) with 4 mm outer diameter and 0.5 mm wall thickness was used as the elastic bladder in both the extensile and contractile chambers. Both chambers also used polyimide braid (Bossert Kast, Germany). Each braid is composed of 48 strands of 0.07 mm diameter polyimide woven together. The contractile chamber braid was woven with a 34.5° angle between the longitudinal axis of the muscle and the orientation of the brain, while the extensile chamber braid was woven with a 60° braid angle. Braid angles were chosen as the highest and lowest available from the manufacturer, to give the widest possible range of motion. Chamber lengths were selected to create equal and opposite amounts of contraction and extension as the actuator is pressurized.

All prototypes were pneumatically sealed and bonded together using Dymax 204-CTH-F UV-cure adhesive. The integrated WCs were made from 1.9 mm to 1.5 mm outer diameter, 0.1 mm wall thickness stainless steel tubing (Salomon's Metalen, Groningen, Netherlands). The 1.9 mm tubing was selected to provide room for a 1.65 mm deflated FETO balloon. When the 1.9 mm prototype showed performance issues as detailed in Sec. 4.2, a 1.5 mm prototype was constructed to provide a proof of concept, which will be improved upon in future designs. Figure 5 shows a fully assembled dual-chamber PAM.

A custom test jig shown in Fig. 7 was used to evaluate the performance of each prototype. The jig includes clamping pieces to hold the prototype in place, a 10 kg load cell (Tedea-Huntleigh model 1022), and a laser distance sensor (model OADM 12I6460/S35A, Baumer, Switzerland). The driving pressure for each prototype is supplied by a proportional pressure regulator (model VEAA, Festo, Germany) and measured by a pressure sensor (PA-21Y, Keller, Germany). A CDAQ-9174 system (National Instruments, Texas, USA) with modules for analog voltage input (NI9205), analog current input (NI9203), analog bridge input (NI9237), and analog voltage output (NI9263) was used to record test results and produce a variable signal for open-loop control of the proportional pressure regulator output. Data acquisition was configured in a custom LabVIEW program as a multi-channel DAQmx task to ensure measurements for all sensors were synched in time.

3. Experiments

The four prototypes were each mounted in the jig shown in Fig. 7 and actuated by variable pressure inputs to evaluate their performance. Two test configurations

J. Med. Robot. Res. 2022.07. Downloaded from www.worldscientific.com
by KATHOLIEKE UNIVERSITEIT LEUVEN on 10/10/22. Re-use and distribution is strictly not permitted, except for Open Access articles.

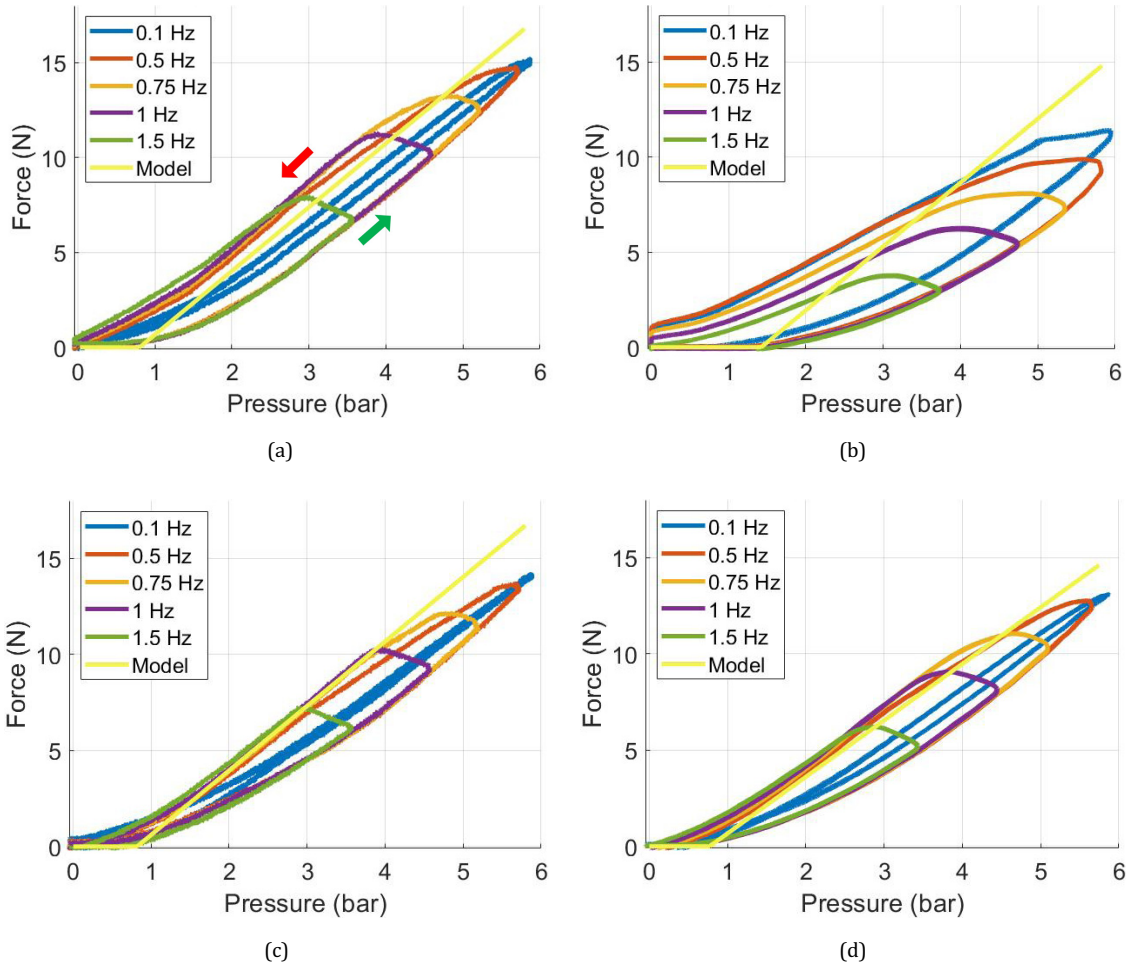

Fig. 8. Prototype characterization showing a comparison of the theoretical modeled and experimentally measured blocked force output at various frequencies for (a) dual-chamber prototype with 1.5 mm diameter WC; (b) dual-chamber prototype with 1.9 mm diameter WC; (c) dual-chamber prototype with no WC, and (d) contractile PAM.

were used. In the first, the traveling attachment point of each prototype was rigidly connected to the load cell in order to characterize the blocked force each PAM was capable of generating. For the second variety of test, the traveling attachment point was allowed to move freely and the distance traveled was recorded by the laser distance sensor. Each prototype was driven by a range of different actuation pressures including sinusoidal waves of variable frequency and step changes in pressure. Similar to several previous studies characterizing miniature PAMs [8, 14], tests were performed over a pressure range of 0–6 bar.

The results of the blocked force testing for each prototype are summarized in Fig. 8, which shows the experimentally measured force generated in response to different frequencies of a sinusoidal pulsed input pressure in comparison to the model predicted force values using (2). The free travel distance test results are reported in Fig. 9. Every force and distance test shown in Figs. 8 and 9 was repeated three times at each frequency, with data from all three repetitions included in each graph. Maximum measured force output, modeled force output, stroke length, and actuator movement speed are listed in Table 1.

3.1. *Evaluation of PAM to drive nitinol bending segment*

In order to assess clinical capability of the prototype PAMs, the 1.5 mm diameter WC dual-chamber PAM was used to actuate a nitinol bending segment as shown in Fig. 12(a). This 3.3 mm diameter, 40 mm long bending segment was selected as the dimensions are similar to the flexible fetoscope geometry defined in Sec. 1.2. As shown in Fig. 12, the muscle was used to actuate the bending segment at different pressures. The tip of the bending segment was then fixed to a force sensor as shown in Fig. 12(e), and actuated to measure the lateral force applied at the tip of the bending segment as seen in Fig. 12(f).

J. Med. Robot. Res. 2022.07. Downloaded from www.worldscientific.com
by KATHOLIEKE UNIVERSITEIT LEUVEN on 10/10/22. Re-use and distribution is strictly not permitted, except for Open Access articles.

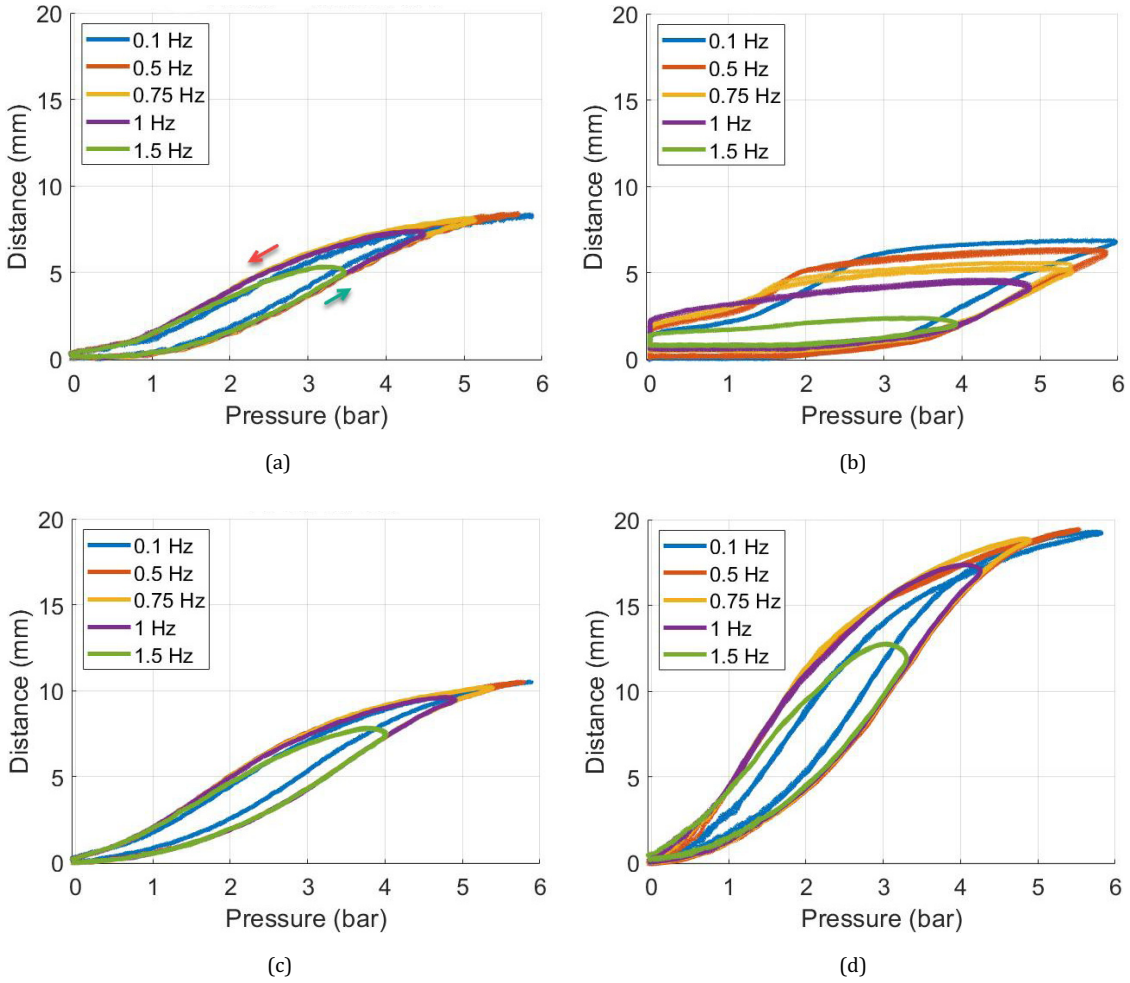

Fig. 9. Prototype characterization showing a comparison of free motion actuator stroke length at various frequencies for (a) dual-chamber prototype with 1.5 mm diameter WC; (b) dual-chamber prototype with 1.9 mm diameter WC; (c) dual-chamber prototype with no WC, and (d) contractile PAM.

Table 1. Prototype characterization — maximum outputs.

Prototype	Max Force — Experimental	Max Force — Modeled	Max Stroke Length	Max Speed
Dual-chamber 1.5 mm WC	15.25 N	16.78 N	8.39 mm, 6.45%	19.1 mm/s
Dual-chamber 1.9 mm WC	11.63 N	14.81 N	6.96 mm, 5.35%	12.65 mm/s
Dual-chamber no WC	14.25 N	16.71 N	10.6 mm, 8.12%	24.1 mm/s
Contractile	13.31 N	14.55 N	19.3 mm, 14.9%	46.1 mm/s

4. Discussion

4.1. *Blocked force and stroke length testing*

Data produced in this study show the basic performance characteristics of several variations of a novel PAM design in comparison to a typical contractile McKibben muscle. As seen in Table 1, the dual-chamber PAM with 1.5 mm integrated WC produced the highest maximum force of any PAM evaluated at 15.25 N, compared to the traditional contractile muscle's maximum force of 13.31 N. This result is in agreement with both modeled results (10% modeling error at maximum pressure for the 1.5 mm WC dual-chamber PAM) and previous experiments such as those performed by Kothera *et al.* [17] which found no significant change in PAM blocked force output as a function of the actuator's length. This implies that the shorter contractile PAM in the dual-chamber prototypes will produce similar force to the longer contractile-only PAM prototype even before the extensile chamber's force contribution is considered. It was also expected based on previously reported results investigating the properties of extensile PAMs that the

J. Med. Robot. Res. 2022.07. Downloaded from www.worldscientific.com
by KATHOLIEKE UNIVERSITEIT LEUVEN on 10/10/22. Re-use and distribution is strictly not permitted, except for Open Access articles.

contractile PAM prototype would be relatively close to the dual-chamber prototypes in force generation, as contractile PAMs have been shown to generate significantly higher output force [12, 23]. The maximum force output contribution of the prototype with 1.5 mm WC's extensile chamber is approximately 2 N, the difference between forces generated by a dual chamber and contraction only PAM in experimental testing. Extensile force and stroke could be increased in future designs by using an extensile chamber braided mesh with higher braid angle. Although only a few prototypes have been built and tested, the initial results suggest that the newly introduced actuator design is capable of achieving a higher actuation force per unit length than traditional McKibben muscles.

As shown in Fig. 9, the contractile PAM produced a significantly higher stroke length than any of the dual-chamber prototypes. This was an expected result and agrees with established theory dating back to Gaylord's 1958 patent [7], in which he proposed a simple equation for the maximum theoretical stroke length of a PAM based on his model relating actuation pressure to PAM force output and the geometry of a PAM's braided mesh. Gaylord predicts that a PAM will reach its maximum stroke length when the force output of the freely contracting or extending PAM has reached 0 N. As shown by Gaylord [7], under these conditions his model predicts the relationship between PAM length (L) and braid strand length (S) as follows:

$$L = S\frac{1}{\sqrt{3}}, \tag{4}$$

where L is the PAM length and S is the length of the strands in the PAM's braided mesh. While this theoretical maximum stroke is unachievable due to friction forces and other simplifying assumptions made by Gaylord's model, it still provides a useful reference when predicting the capabilities of PAM prototypes. Because the theoretical maximum PAM stroke is expected to vary just as a function of braid length, and the braid length of the contractile PAM prototype must always be longer than the braid length of the contractile chamber of an equal-length dual-chamber PAM, an actuator configured as a pure contractile or extensile PAM should always achieve a larger maximum stroke length than a dual-chamber PAM.

4.2. *Prototyping challenges, design benefits, and PAM safety*

During testing of the dual-chamber prototype with 1.9 mm WC it was observed that there was significant interference between the elastic bladder of the extensile chamber and the outer surface of the WC. This interference was significant enough to prevent the actuator from fully returning to its resting position during high frequency actuations, as seen in Fig. 9(b). As the extensile chamber extends axially it also contracts radially. This brought the silicone bladder into contact with the stainless steel tubing, accounting for the more significant hysteresis, higher dead-band pressure, and lower maximum values achieved by the 1.9 mm WC prototype as seen in Figs. 8(b) and 9(b). No similar behavior was visually observed during testing for the 1.5 mm WC prototype, although the slightly lower stroke length when compared to the dual-chamber prototype with no WC suggests that there may still be some interference, adding friction between the silicone bladder and stainless steel tubing and preventing the actuator from achieving full stroke length.

Several potential methods could be used to prevent this interference issue in future prototypes. Given the inherent configurability of the dual-chamber design, it is possible to selectively tune the material components and geometry of each chamber independently, expanding the available options to tailor design of a dual-chamber actuator for use in highly constrained performance-critical applications. Reducing the WC outside diameter from 1.9 mm to 1.5 mm was shown to greatly reduce hysteresis in the actuator response and increase overall force output and stroke length. In applications where a large WC is critical it would be possible to lubricate the interior of the extensile chamber during construction or select more lubricious materials for the elastic bladder and WC. Future designs could also use a larger diameter or thinner wall thickness elastic bladder for the extensile chamber to increase the starting distance between the elastic bladder and WC. In applications where a long stroke length is not critical the initial lengths of the chambers could be adjusted to minimize the extent that the extensile bladder radially contracts. Stroke length and force output of the extensile chamber could be increased by using a braided mesh with higher braid angle, although this will likely increase radial contraction and so the chance of interference between the bladder and WC. Many of these modifications should be possible with minimal effect on the contractile chamber's contribution to actuator output.

All PAM prototypes evaluated in this study showed significant hysteresis characteristics as a function of actuation pressure frequency as shown in Figs. 8 and 9. With the exception of results for the 1.9 mm WC prototype (particularly Fig. 9(b)), force and stroke length output results were highly repeatable, with all three tests per frequency displayed in Figs. 8 and 9 largely indistinguishable. As discussed previously, interference between the elastic bladder and WC of the 1.9 mm WC prototype caused some significant hysteresis at all frequencies tested. Test results for all other prototypes showed moderate hysteresis at frequencies of 0.1 Hz and below. The hysteresis envelope became more pronounced between 0.1 Hz and 1.0 Hz for these prototypes.

J. Med. Robot. Res. 2022.07. Downloaded from www.worldscientific.com
by KATHOLIEKE UNIVERSITEIT LEUVEN on 10/10/22. Re-use and distribution is strictly not permitted, except for Open Access articles.

Note that at higher frequencies the full 6 bar of pressure requested by the controller was not reached. This suggests that the decreased maximum force output and stroke length in high frequency tests is likely limited by the flow rate of the proportional pressure regulator.

4.3. *Model performance evaluation*

The theoretical model used in this study gave a reasonable prediction of actuator force output, as shown in Fig. 10, which shows modeled force output, experimentally measured force, and modeling error (absolute value in Newtons) for a 0.5 Hz sinusoidal pressure input. The 0.5 Hz data set was selected for comparison as the fastest frequency tested which did not show significant rate-dependent hysteresis. Modeling error for the 1.5 mm WC prototype ranged from 0 N to 3.18 N or 0–21% of maximum response (Fig. 10(a)), and from 0 N to 3.21 N or 0–23.2% of maximum response for the contractile prototype (Fig. 10(d)). The model tended to overestimate force output, especially in the rising portion of the cycle and at higher input frequencies. The model also does not account for hysteresis in the actuator response, making it less suitable to predict the output of high frequency signals. In Fig. 10(b), the 1.9 mm WC prototype displays the previously discussed elastic bladder–WC interference issue, with the actuator not returning fully to resting position within 1.5 s of actuation. Future studies should investigate performing quasi-static response testing to characterize the stress and strain responses of these PAMs across their dynamic range. Quasi-static testing has

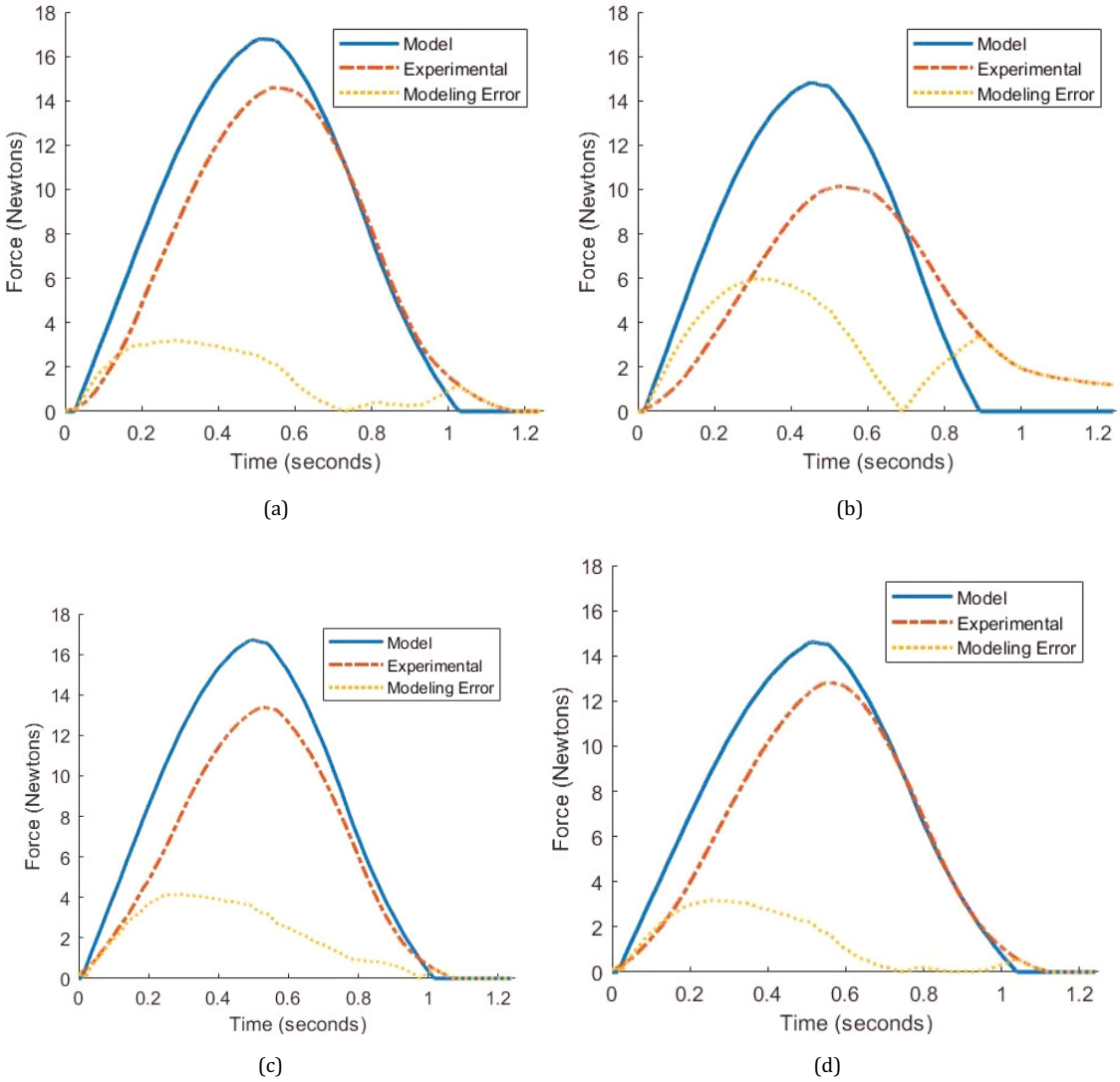

Fig. 10. Comparison between theoretically modeled force output, experimentally measured forces, and modeling error (absolute value in Newtons) for (a) dual-chamber prototype with 1.5 mm diameter WC; (b) dual-chamber prototype with 1.9 mm diameter WC; (c) dual-chamber prototype with no WC, and (d) contractile PAM. All data based on one test of a pulsed sinusoidal pressure input at 0.5 Hz.

J. Med. Robot. Res. 2022.07. Downloaded from www.worldscientific.com
by KATHOLIEKE UNIVERSITEIT LEUVEN on 10/10/22. Re-use and distribution is strictly not permitted, except for Open Access articles.

been used in several cases to produce highly accurate PAM output models [12, 17, 24, 25], but was not selected for this study in hopes that a more widely applicable theoretical model could be used to characterize prototype output using easily available design parameters (such as bladder and braid geometry and material properties) that would be useful for the design of future prototypes. In order to more accurately model the actuator output behavior across a range of frequencies rate-dependent modeling techniques could be considered based on traditional [26] or artificial intelligence-inspired methods [27].

4.4. *Prototype response speed testing*

Experiments were performed to characterize the response of the prototypes to a rapid change in input pressure, as shown in Fig. 11. This test was first done using an input pressure driven by the proportional pressure regulator. As shown in Fig. 11(a) this resulted in a pressure that ramped from 0 bar to 6 bar over a period of 0.5–0.6 s, and showed little differentiation between prototype responses. This suggests that the response speed is largely limited by the bandwidth of the proportional pressure regulator. A second test was performed with the proportional pressure regulator removed from the pneumatic supply line. Actuation pressure was driven manually by directly connecting the actuator supply line to a 6 bar pressure source via a hand-operated valve. As shown in Fig. 11(b), this resulted in a pressure that ramped from 0 bar to 6 bar over a period of 0.1 s, but there was still little variation observed in the response speed of different prototypes. It was expected that a difference in movement speed would be visible because of the difference in internal volume between prototypes with and without extensile segments and concentric WCs, but a higher flow rate pressure source will be needed to investigate this further. This test still demonstrates the high bandwidth of the prototype PAMs constructed, one of the important characteristics that makes pneumatic actuators desirable for the development of responsive robotic instrumentation.

4.5. *Evaluation of prototype-actuated nitinol tool guide*

In order to evaluate the proposed PAM design in a clinically relevant setting, we combined the prototype PAM with a nitinol tool guide designed for use in a flexible fetoscopic device (see Fig. 12(a)), and assessed the bending capability and tip force generated during actuation. This experimental configuration is intended to mimic the case illustrated in Fig. 4(e), in which the actuator is built into the surgical device's handpiece and transmits force to the bending segment via a cable. The PAM was able to actuate the one DOF uniaxial bending segment over a range of 0–80° using an input pressure of 0–6 bar. The distal tip force produced was a maximum of 0.67 N, as seen in Fig. 12(f). This lateral tip force is relatively small in comparison to the direct pull force of the PAM due to the short moment arm on which the PAM pulls to actuate the segment. In general for MIS devices a large lateral tip force is beneficial for load-bearing tasks that must be performed at the surgical site (e.g. repositioning the mouth of a fetus, moving the fetal tongue, or needle driving in other MIS applications), while a low blocked lateral tip force during actuation helps to ensure that excessive forces are not unintentionally transmitted to delicate anatomy. Future work should be done to optimize the device lateral tip force by modifying the cutting pattern that defines the tool guide's mechanical properties.

This experiment shows that the current PAM prototype is capable of actuating a bending segment that fits the design requirements introduced in Sec. 1.2. This bending segment design and prototype PAM would be

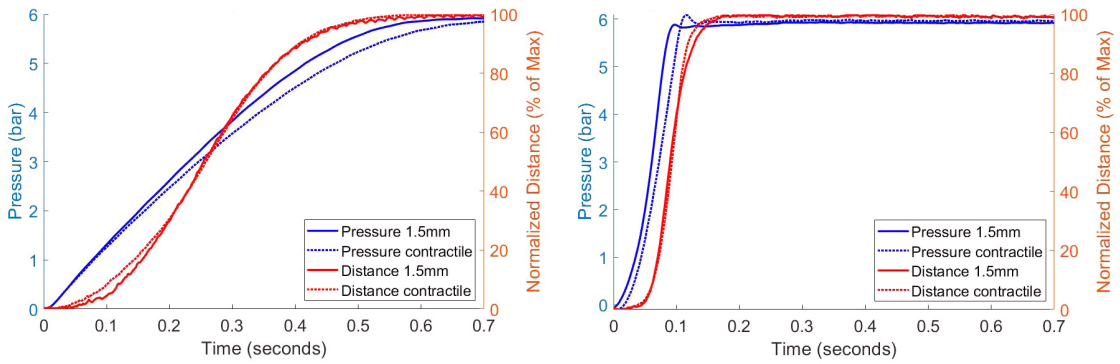

Fig. 11. Actuator stroke in response to a rapid change in input pressure driven by (a) actuation pressure supplied by the proportional pressure regulator and (b) actuation pressure supplied by direct connection to a 6 bar pressure supply. Stroke length normalized to maximum stroke per prototype.

J. Med. Robot. Res. 2022.07. Downloaded from www.worldscientific.com
by KATHOLIEKE UNIVERSITEIT LEUVEN on 10/10/22. Re-use and distribution is strictly not permitted, except for Open Access articles.

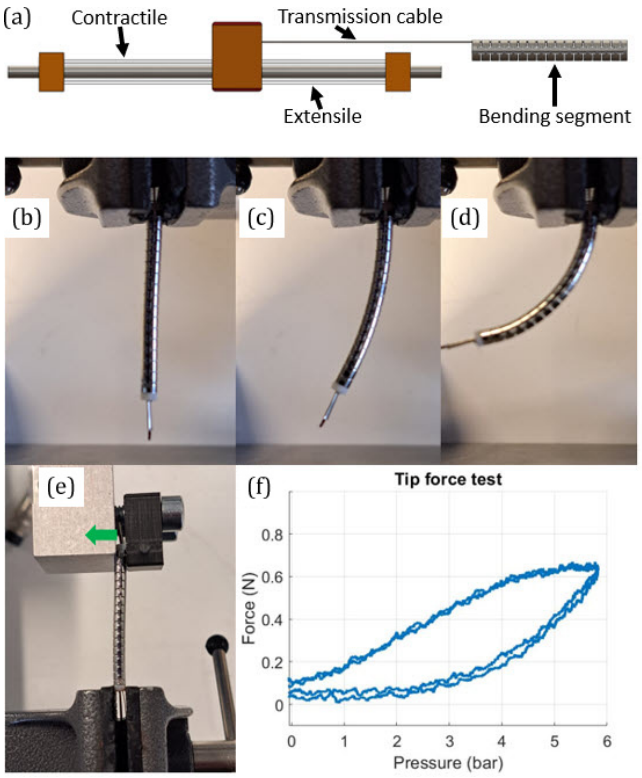

Fig. 12. Figure showing (a) the nitinol bending segment attached to a dual-chamber concentric PAM, (b) bending segment at rest, (c) bending segment actuated with 3 bar of pressure, (d) bending segment actuated with 6 bar of pressure, (e) bending segment fixed to measure distal tip force, with force direction shown by green arrow, and (f) graph of force produced at device tip by PAM actuation.

suitable for development of a fetoscope built around a dual-chamber PAM embedded in the handle actuating the device tip via a tendon as seen in Fig. 12(a). The actuation performance of the current prototype also demonstrates the viability of developing a miniaturized combination bending segment and PAM as shown in Fig. 4(e) for use in a flexible fetoscope.

4.6. *Pneumatic safety, design benefits, and future direction*

An important aspect of designing a pneumatically actuated flexible fetoscope is ensuring that steps are taken to minimize the risk of harm to the patient in the event of a pneumatic leak or bladder rupture. The range of driving pressures investigated in this study (0–6 bar) is comparable to the range of pressures used in cardiac surgery devices such as the True Flow Valvuloplasty Perfusion Catheter (Becton Dickinson, USA) which uses balloons pressurized to 3–6 atm in close proximity to fragile cardiac patient anatomy. The proposed integrated design shown in Fig. 4 protects the pneumatic chamber from direct contact with any sharp instruments in the surgical field by embedding the chambers in a nitinol tool guide. To further mitigate risk of damage in the event of a leak it would be possible to restrict the pressurized volume attached to the actuator (such as by using a small pressurized canister to drive actuation, or by monitoring media pressure and flow rate and activating a relief valve safely away from the patient if a leak is detected). Additionally a pressurization medium such as phosphate buffered saline could be used to minimize the risk of tissue damage in the event of a leak inside the womb or fetal trachea. Given the available mitigation strategies, it is not expected that the use of a shaft-embedded PAM in a flexible fetoscope will pose a risk to fetus, mother, or surgeon.

A flexible MIS instrument actuated by a shaft-embedded PAM offers several advantages when compared to state-of-the-art surgical devices which typically transmit actuation force to flexible appendages via drive cables. The shaft-embedded PAM will apply energy directly at the point of motion, eliminating any risk of parasitic bending caused by transmission cables exerting force on device walls in unintended places. An embedded PAM also offers advantages in modularization, needing only a pneumatic supply to be passed through an articulating segment instead of a rigid cable. These properties could be used to develop more accurate high DOF instruments with multiple bending segments in series to access more remote anatomy. Removing the need for a cable transmission system could also improve device longevity, by eliminating cable wear as a mode of failure. This could enable development of longer-lasting reusable robotic surgery actuators, reducing system cost compared to the current state of the art. While designing PAM-based MIS instruments does introduce several new technical challenges, the potential benefits are significant enough to merit further investigation.

Future work should be done to optimize the concentric dual-chamber actuator design for use in miniature surgical instrumentation for robot-assisted MIS procedures. The current prototype actuators with 4 mm diameter chambers could be used in a flexible fetoscope design with a handle-based actuator and cable-driven tip as shown in Fig. 4(e). The anticipated minimum length of a handle built using the prototype tested in the study would be approximately 150 mm, with minimum outer diameter of 10 mm. The prototype actuator would add only 4.1 g of weight to the device. These parameters could be tuned further to optimize the ergonomics. To produce a device based on a shaft-embedded actuator, further miniaturization will be needed to develop chambers that can fit within the 3.3 mm footprint (requirement 1.2.2) without interfering with a WC for a 1.75 mm diameter balloon (1.2.3) as specified in the design requirements listed in Sec. 1.2. The current PAM prototype was capable of actuating a 40 mm length bending arm over 80° of bending. This is near

J. Med. Robot. Res. 2022.07. Downloaded from www.worldscientific.com
by KATHOLIEKE UNIVERSITEIT LEUVEN on 10/10/22. Re-use and distribution is strictly not permitted, except for Open Access articles.

the 90° of bending laid out in the fetoscope design requirements (1.2.4), and can be further improved by optimizing the geometry of the bending tool guide to allow additional motion using the PAMs force output. The low tip forces seen in Fig. 12(f) demonstrate the current prototype's safety for use in maneuvering past delicate tissues to reach the fetal throat (1.2.5a), while the bending segment's rigidity in the nonbending axis will need to be optimized and evaluated in future miniaturized designs (1.2.5b). The remaining design requirements (1.2.1 — must provide visualization and capabilities equivalent to the state of the art and 1.2.6 — must enable fetal trachea access from a wider range of initial incisions) require the integration of additional device components for a meaningful evaluation, and so will be considered in future work focused on building a full flexible fetoscope around the actuator design introduced in this paper.

5. Conclusion

This paper presented the design of a novel miniature pneumatic actuator with integrated WC for use in flexible robotic instrumentation. Several variations of this design were built and their performance was evaluated in comparison to a traditional contractile McKibben muscle. A theoretical model for force output of the novel actuator was proposed and compared to experimental results. One key challenge in the current design was identified (the issue of interference between the elastic bladder and WC), with solutions proposed to resolve this issue in future design iterations. The initial results reported in this study suggest that the novel actuator design is capable of producing more force per unit actuator length than a traditional McKibben muscle, at the cost of a smaller stroke length per unit actuator length. The proposed design shows promise for future miniaturization and refinement for integration into flexible robotic instrumentation for MIS procedures. Future work should focus on solving the elastic bladder–WC interference issue, improving output model accuracy across all actuation pressure signal frequencies, and optimizing design of the contractile and extensile chambers for integration with a flexible fetoscope that meets the design requirements outlined in Sec. 1.2 of this paper.

Acknowledgment

This project received funding from the FLEXFET project (3E200384), an internally funded C2 project of KU Leuven.

References

1. J. Deprest, K. Nicolaides, E. Benachi, A. Gratacos, G. Ryan, N. Persico, H. Sago, A. Johnson, M. Wielgos, C. Berg, B. Van Calster and F. Russo, Randomized trial of fetal surgery for severe left diaphragmatic hernia, *N. Engl. J. Med.* **385** (2021) 107–118.
2. J. A. Jiménez, E. Eixarch, P. Dekoninck, J. R. Bennini, R. Devlieger, C. F. Peralta, E. Gratacos and J. Deprest, Balloon removal after fetoscopic endoluminal tracheal occlusion for congenital diaphragmatic hernia, *Am. J. Obstet. Gynecol.* **217**(1) (2017) 78.
3. S. G. Petersen, K. S. Gibbons, F. I. Luks, L. Lewi, A. Diemert, K. Hecher, J. E. Dickinson, J. J. Stirnemann, Y. Ville, R. Devlieger, G. Gardener and J. Deprest, The impact of entry technique and access diameter on prelabour rupture of membranes following primary fetoscopic laser treatment for twin-twin transfusion syndrome, *Fetal Diagn. Ther.* **40**(2) (2016) 100–109.
4. M. De Volder, A. Moers and D. Reynaerts, Fabrication and control of miniature McKibben actuators, *Sens. Actuators A, Phys.* **166**(1) (2011) 111–116.
5. B. Woods, M. Gentry, C. Kothera and N. Wereley, Fatigue life testing of swaged pneumatic artificial muscles for aerospace morphing applications, *J. Intell. Mater. Syst. Struct.* **23** (2012) 327–343.
6. R. Hoggett, 1957-artificial muscle-Joseph laws McKibben (2012), cyberneticzoo.com/bionics/.
7. R. Gaylord, Fluid actuated motor system and stroking device, U.S. Patent 2,844,126 (1958).
8. A. Moers, M. De Volder and D. Reynaerts, Integrated high pressure microhydraulic actuation and control for surgical instruments, *Biomed. Microdevices* **14**(4) (2012) 699–708.
9. D. Sangian, S. Naficy, G. M. Spinks and B. Tondu, The effect of geometry and material properties on the performance of a small hydraulic McKibben muscle system, *Sens. Actuators A, Phys.* **234** (2015) 150–157.
10. B. Tondu, S. Ippolito, J. Guiochet and A. Daidie, A seven-degrees-of-freedom robot-arm driven by pneumatic artificial muscles for humanoid robots, *Int. J. Robot. Res.* **24**(4) (2005) 257–274.
11. W. Liu and C. Rahn, Fiber-reinforced membrane models of McKibben actuators, *J. Appl. Mech.* **70**(6) (2003) 853–859.
12. J. Garbulinski, S. C. Balasankula and N. M. Wereley, Characterization and analysis of extensile fluidic artificial muscles, *Actuators* **10**(2) (2021) 26.
13. W. McMahan, V. Chitrakaran, M. Csencsits, D. Dawson, I. Walker, B. Jones, M. Pritts, D. Dienno, M. Grissom and C. Rahn, Field trials and testing of the OctArm continuum manipulator, in *Proc. 2006 IEEE Int. Conf. Robotics and Automation, 2006. ICRA 2006* (IEEE, 2006), pp. 2336–2341.
14. J. Legrand, M. Ourak and E. B. Vander Poorten, Concentric muscles – Miniature pneumatic actuator with integrated channel for surgical instruments, in *ACTUATOR; Int. Conf. Exhibition on New Actuator Systems and Applications 2021* (VDE, 2021), pp. 1–4.
15. R. Lathrop, M. Ourak, F. Russo, J. Deprest and E. B. Vander Poorten, Design and characterization of a miniature dual-chamber pneumatic actuator for minimally invasive surgical devices, in *2021 Int. Symp. Medical Robotics* (IEEE, 2021), pp. 1–5.
16. G. K. Klute and B. Hannaford, Accounting for elastic energy storage in McKibben artificial muscle actuators, *J. Dyn. Syst. Meas. Control* **122** (1998) 386–388.
17. C. S. Kothera, M. Jangid, J. Sirohi and N. M. Wereley, Experimental characterization and static modeling of McKibben actuators, *J. Mech. Des.* **131**(9) (2009) 091010.
18. C.-P. Chou and B. Hannaford, Measurement and modeling of McKibben pneumatic artificial muscles, *IEEE Trans. Robot. Autom.* **12** (1996) 90–102.
19. T. E. Pillsbury, C. S. Kothera and N. M. Wereley, Effect of bladder wall thickness on miniature pneumatic artificial muscle performance, *Bioinspiration Biomimetics* **10** (2015) 055006.

20. E. Kelasidi, G. Andrikopoulos, G. Nikolakopoulos and S. Manesis, A survey on pneumatic muscle actuators modeling, in *2011 IEEE Int. Symp. Industrial Electronics* (IEEE, 2011), pp. 1263–1269.
21. V. M. Tri, B. Kamers, H. Ramon and H. V. Brussel, Characterization of hysteresis in a pneumatic muscle manipulator with accounting for the creep effect, *IFAC Proc. Vol.* **43**(21) (2010) 296–302.
22. B. Tondu, Modelling of the McKibben artificial muscle: A review, *J. Intell. Mater. Syst. Struct.* **23**(3) (2012) 225–253.
23. T. E. Pillsbury, Q. Guan and N. M. Wereley, Comparison of contractile and extensile pneumatic artificial muscles, in *2016 IEEE Int. Conf. Advanced Intelligent Mechatronics (AIM)* (IEEE, 2016), pp. 94–99.
24. E. G. Hocking and N. M. Wereley, Analysis of nonlinear elastic behavior in miniature pneumatic artificial muscles, *Smart Mater. Struct.* **22** (2012) 014016.
25. M. A. Meller, M. Bryant and E. Garcia, Reconsidering the McKibben muscle: Energetics, operating fluid, and bladder material, *J. Intell. Mater. Syst. Struct.* **25**(18) (2014) 2276–2293.
26. S. Shakiba, M. Ourak, E. Vander Poorten, M. Ayati and A. Yousefi-Koma, Modeling and compensation of asymmetric rate-dependent hysteresis of a miniature pneumatic artificial muscle-based catheter, *Mech. Syst. Signal Process.* **154** (2021) 107532.
27. D. Wu, Y. Zhang, M. Ourak, K. Niu, J. Dankelman and E. Vander Poorten, Hysteresis modeling of robotic catheters based on long short-term memory network for improved environment reconstruction, *IEEE Robot. Autom. Lett.* **6**(2) (2021) 2106–2113.

Robert Lathrop received his ME and BSE degrees in Biomedical Engineering from the University of Cincinnati in 2013 and the Tulane University in 2012, respectively. From 2013 to 2020, he worked as Research Engineer for Smith and Nephew developing electrosurgical devices and robotic systems for sports medicine and orthopedics applications. He is pursuing PhD at the Katholieke Universiteit Leuven in the Robot-Assisted Surgery group. His research interests include surgical robotics, sensing and control of continuum robots, and medical device design.

Mouloud Ourak holds PhD in Automation and Robotics from Université de Franche-Comté in 2016 and MS degree in Robotics and Vision from Université de Montpellier in 2013, in France. Since 2017, he is with the Katholieke Universiteit Leuven in the MECH department at RAS group as Postdoctoral Researcher (Leuven, Belgium). Currently, his research activities are related to surgical robotics (actuators and control laws), vision, and visual serving.

Jan Deprest, MD PhD FRCOG, is Professor of Obstetrics and Gynaecology at the KU Leuven (Belgium) and the UCL (United Kingdom). He has a research interest in fetal surgery, in particular to antenatal interventions that modulate fetal development in case of congenital birth defects. He directs the clinical fetal surgery program in Leuven, and did setup the program at the University College London Hospital to treat fetuses with spina bifida and congenital diaphragmatic hernia. Both teams are working on novel image-guided surgical instruments for fetal surgery. He initiated and directed the Eurofoetus consortium, which designed a series of fetoscopic instruments with support from the European Commission, and since a number of other European projects in fetal medicine. He published over 700 peer reviewed papers, and directed over 30 PhD projects. He has been awarded the Haackert foundation gold medal (2015), the ISUOG Ian Donald Award (2018), and the J Daels prize by the Belgian Royal Academy of Medical Sciences. He is *fellow ad eundem* from the RCOG.

Emmanuel Vander Poorten received BS degree in Mechanical Engineering in 2000 from the University of Leuven, Belgium. He obtained the title of Doctor in Engineering in May 2007, from the Kyoto University, Japan. Currently, he is Associate Professor at the Faculty of Engineering Technology and the Mechanical Engineering Department of the University of Leuven. His research interests include surgical robotics, sensing and control for continuum robots, medical device design, human–robotic interaction, shared control, haptic interfacing, and teleoperation.

J. Med. Robot. Res. 2022.07. Downloaded from www.worldscientific.com
by KATHOLIEKE UNIVERSITEIT LEUVEN on 10/10/22. Re-use and distribution is strictly not permitted, except for Open Access articles.